

Signals of a superlight gravitino at the LHC

Fabio Maltoni,^a Antony Martini,^a Kentarou Mawatari^b and Bettina Oehl^b

^a*Centre for Cosmology, Particle Physics and Phenomenology (CP3),
Université catholique de Louvain, Chemin du Cyclotron 2, B-1348 Louvain-la-Neuve, Belgium*

^b*Theoretische Natuurkunde and IIHE/ELEM, Vrije Universiteit Brussel,
and International Solvay Institutes, Pleinlaan 2, B-1050 Brussels, Belgium*

E-mail: fabio.maltoni@uclouvain.be, antony.martini@uclouvain.be,
kentarou.mawatari@vub.ac.be, bettina.oehl@vub.ac.be

ABSTRACT: Very light gravitinos could be produced at a sizeable rate at colliders and have been searched for in the mono-photon or mono-jet plus missing momentum signature. Strategies for enhancing the signal over background and interpretations of the experimental results are typically obtained within an effective field theory approach where all SUSY particles except the gravitino are heavy and are not produced resonantly. We extend this approach to a simplified model that includes squarks and gluinos in the TeV range. In such a case, the jet(s)-plus-missing-momentum signature can be generated through three different concurring mechanisms: gravitino-pair production with an extra jet, associated gravitino production with a squark or a gluino, or squark/gluino pair production with their subsequent decay to a gravitino and a jet. By using a matrix-element parton-shower merging procedure, we take into account all the relevant production processes consistently, explore the SUSY parameter space with the LHC Run-I data set, and give prospects for the Run II. We also consider the reach of other signatures involving electroweak particles, e.g., the mono-photon, $-Z$, or $-W$ plus missing momentum. The current mono-jet and mono-photon LHC analyses are interpreted to set a lower bound on the gravitino mass. We show how the limit of $m_{3/2} > 1.7 \times 10^{-13}$ GeV obtained in the effective field theory hypothesis is modified when the squarks and/or the gluino are in the TeV range.

Contents

1	Introduction	1
2	Light gravitino production at the LHC	3
2.1	SUSY QCD with a goldstino superfield	3
2.2	Light gravitino production	5
2.2.1	Gravitino pair production	6
2.2.2	Associated gravitino production	6
2.2.3	Indirect gravitino production	7
2.3	Event simulation tools	8
3	Mono-jet plus missing momentum	8
3.1	Total rates	9
3.2	Differential distributions	10
3.3	Recasting LHC mono-jet analyses	11
3.3.1	Selection cuts	13
3.3.2	Merging matrix elements with parton showers	14
3.3.3	Limit on the gravitino mass	15
4	Mono-photon, $-Z$, or $-W$ plus missing momentum	16
5	Summary	19

1 Introduction

Events with large missing momentum, and in particular those featuring just one visible recoiling object (a jet, a photon, a weak boson, a top quark), are among the most promising final states where to look for signs of new physics at colliders. Their simplicity and model independent nature appeal to both theorists and experimentalists. There are, however, important challenges that have to be faced with such signatures. The first ones are of experimental nature. The accurate and precise determination of the missing momentum in events needs a detailed control of many aspects, from triggering to jet energy scales, to underlying event simulation, to pile-up mitigation. In addition, in case of weak boson or top quark, tagging and reconstruction efficiencies for the recoiling object(s) also enter. The second class of challenges are more of theoretical nature and have to do with the problem of maximising the information that can be extracted from data to constrain new physics models. Model-independent searches for dark matter (DM) constitute the most popular interpretations of mono-jet analyses at the LHC, both in an effective field theory (EFT) framework as well as in simplified models, see e.g. [1–3] and the references therein.

Among new complete physics scenarios leading to mono-object plus large missing momentum signals, supersymmetric (SUSY) models with a very light (or *superlight*) gravitino play a special role: they offer a concrete setting where the strengths and limitations of EFT approach vis-a-vis more UV completed models can be studied in detail.

Let us look closer at model constraints from mono-object searches at previous and current colliders. At the LEP collider, the mono-photon signal was used to set a limit on models of SUSY with the gravitino as the lightest SUSY particle (LSP) and extra dimensions [4–7]. In some SUSY scenarios the gravitino can be very light of order $m_{3/2} \sim \mathcal{O}(10^{-14} - 10^{-12})$ GeV with all the other SUSY particles being above the TeV threshold [8, 9]. We dub such a scenario as “*gravitino EFT*”. The only relevant parameter in this case is the gravitino mass, which is directly related to the SUSY breaking scale, the lower limit being $m_{3/2} > 1.35 \times 10^{-14}$ GeV [6, 10]. Alternatively, we consider the gravitino LSP in the minimal supersymmetric standard model (MSSM) with other sparticles at the TeV scale. In this scenario, the process of the neutralino–gravitino associated production with the subsequent neutralino decay into a photon and a gravitino has been used to put a limit on the gravitino mass as a function of the neutralino and selectron masses [11–16], e.g. $m_{3/2} \gtrsim 10^{-14}$ GeV for $m_{\tilde{\chi}_1^0} = 140$ GeV and $m_{\tilde{e}} = 150$ GeV [7]. Such a scenario can also be considered as a simplified SUSY model, where only the gravitinos, the lightest neutralino and the selectrons play a role in the phenomenology at colliders.

At the Tevatron, not only the mono-photon but also the mono-jet signals constrain models of SUSY [17, 18] and extra dimensions [18–20]. Similar to the LEP bound, in the gravitino-EFT limit [21] a gravitino is excluded below 1.1×10^{-14} GeV and 1.17×10^{-14} GeV in the mono-jet [17] and mono-photon [18] channels, respectively.

At the LHC, besides the mono-photon [22, 23] and mono-jet [24, 25] signals, other mono-object plus missing transverse momentum signals such as a Z boson [26], a lepton [27, 28], and a top quark [29] have been investigated mostly in the context of DM searches and more exotic models. SUSY models have been considered only in the ATLAS mono-jet analysis [24], where the gluino–gravitino [30–35] and squark–gravitino [33, 34] associated productions were taken into account to set a limit on the gravitino mass as a function of the squark and gluino masses as, e.g.

$$m_{3/2} > 1 \times 10^{-13} (4 \times 10^{-14}) \text{ GeV} \quad (1.1)$$

for the degenerate squark and gluino masses at $m_{\tilde{q}, \tilde{g}} = 500$ (1700) GeV. One point that is relevant for this work is that the above limit may be modified by the contribution from the direct gravitino-pair production in association with an extra jet, a production channel so far disregarded in the analysis. Moreover, while event selection is targeted to the associated gravitino production, events from squark and gluino pair production may enter the signal region affecting the results.

We would like to put forward the interpretation of the mono-object signals in the SUSY context with a very light gravitino for the LHC. As mentioned above, extending the gravitino EFT to the full MSSM (or simplified SUSY models), other production channels can contribute leading to rather different final state features that in turn depend on the SUSY parameters. In Ref. [36] we studied the gluino–gravitino and gluino-pair production

in this very same context. However, the gravitino-pair production associated with a jet and squark-gravitino production were not included there. In this work we present, for the first time, the complete set of production channels consistently treated in a unique framework that can provide accurate predictions for the general case. In addition, although the gravitino in our scenario is too light to be a cold DM candidate, the approach we have followed is fully general and can be used as a template for passing from an EFT approach to simplified models in the context of DM searches [37].

The plan of the paper is as follows. In sec. 2 we focus on the SUSY QCD sector in order to assess the parameter space relevant for gravitino production processes and potentially contributing to the mono-jet signature. We explicitly construct a SUSY QCD model in sec. 2.1. In sec. 2.2 we present the three different yet related mechanisms which produce gravitinos. Gravitino-pair production with one jet has been studied in the gravitino-EFT limit only [21], where exact tree-level results for $2 \rightarrow 3$ matrix elements for $p\bar{p}/pp \rightarrow \tilde{G}\tilde{G}j$ have been computed only for the quark-antiquark and quark-gluon initial states, but not for gluon-gluon ones. We obtain such results for generic squark/gluino masses and for all processes for the first time in this work. In sec. 2.3 we briefly review the computation/simulation tools used in this article. In sec. 3 we study all the relevant gravitino production processes in detail for total as well as differential cross sections. As an application of our results, we recast the ATLAS mono-jet analysis [24] with inclusive signal samples by merging matrix elements with parton showers (ME+PS) in order to set a limit on the masses of the SUSY particles. We suggest improvements to the analysis so to increase the sensitivity to the gravitino mass when squarks and gluinos are light. In sec. 4, we consider the associated production with an electroweak (EW) particle, and study the mono-photon, $-Z$ and $-W$ signals in the very light gravitino context. Finally, we recast the mono-photon analyses at the LHC [22, 23] to set a limit on the gravitino mass. Section 5 is devoted to our conclusions.

2 Light gravitino production at the LHC

In this section we start by constructing a SUSY QCD model by using the superspace formalism. We then present the three mechanisms of light gravitino production at hadron colliders and finally we briefly describe the simulation tools we employ for our results.

2.1 SUSY QCD with a goldstino superfield

In phenomenologically viable SUSY models, SUSY breaking is often assumed to take place in a so-called hidden sector, and then transmitted to the visible sector (i.e. the SM particles and their superpartners) through some mediation mechanism, e.g. gauge mediation or gravity mediation. As a result, one obtains effective couplings of the fields in the visible sector to the goldstino multiplet. To illustrate the interactions among the physical degrees of freedom of the goldstino multiplet and the fields in the visible sector, we introduce an R -parity conserving $N = 1$ global supersymmetric model with the $SU(3)_C$ gauge group in the superspace formalism. The model comprises one vector superfield $V = (A^\mu, \lambda, D_V)$, describing a gluon A^μ and a gluino λ , and two chiral superfields $\Phi_L = (\tilde{q}_L, q_L, F_L)$ and

$\Phi_R = (\tilde{q}_R^*, q_R^c, F_R)$, containing the left- and right-handed quarks $q_{L/R}$ and squarks $\tilde{q}_{L/R}$, where the color and generation indices are suppressed. In addition, we introduce a chiral superfield in the hidden sector $X = (\phi, \tilde{G}, F_X)$, containing a sgoldstino ϕ and a goldstino \tilde{G} . $D_V, F_{L/R}$ and F_X are auxiliary fields.

The Lagrangian of the visible sector is

$$\mathcal{L}_{\text{vis}} = \sum_{i=L,R} \int d^4\theta \Phi_i^\dagger e^{2g_s V} \Phi_i + \left(\frac{1}{16g_s^2} \int d^2\theta W^\alpha W_\alpha + \text{h.c.} \right), \quad (2.1)$$

where g_s is the strong coupling constant.¹ $W_\alpha = -\frac{1}{4} \bar{D} \cdot \bar{D} e^{-2g_s V} D_\alpha e^{2g_s V}$ denotes the SUSY $SU(3)_C$ field strength tensor with D being the superderivative. \mathcal{L}_{vis} contains the kinetic terms as well as the gauge interactions.

The Lagrangian of the goldstino part is given by

$$\mathcal{L}_X = \int d^4\theta X^\dagger X - \left(F \int d^2\theta X + \text{h.c.} \right) - \frac{c_X}{4} \int d^4\theta (X^\dagger X)^2. \quad (2.2)$$

The first term gives the kinetic term of the sgoldstino and the goldstino, while the second term is a source of SUSY breaking and $F \equiv \langle F_X \rangle$ is a vacuum expectation value (VEV) of F_X .² The last term is non-renormalizable and provides interactions in the goldstino multiplet. In addition, this term also gives the sgoldstino mass term when replacing the auxiliary fields F_X by the VEV, and hence we assign $c_X = m_\phi^2/F^2$.

The effective Lagrangian that leads to the interactions among the (s)goldstinos and the fields in the visible sector as well as the soft mass terms for the squarks and the gluinos is given by

$$\mathcal{L}_{\text{int}} = - \sum_{i=L,R} c_{\Phi_i} \int d^4\theta X^\dagger X \Phi_i^\dagger \Phi_i - \left(\frac{c_V}{16g_s^2} \int d^2\theta X W^\alpha W_\alpha + \text{h.c.} \right), \quad (2.3)$$

where we identify $c_{\Phi_i} = m_{\tilde{q}_i}^2/F^2$ and $c_V = 2m_\lambda/F$. We note that our model is minimal, yet enough to generate all the relevant interactions involving two goldstinos in the final state for the jet(s)+ \cancel{E}_T signal at hadron colliders. The extension of the model including the SM electroweak (EW) gauge group is straightforward, and we will study mono- γ , $-W$ and $-Z$ signals later.

Let us briefly refer to the goldstino equivalence theorem. When the global SUSY is promoted to the local one, the goldstino is absorbed by the gravitino via the so-called super-Higgs mechanism. In the high-energy limit, $\sqrt{s} \gg m_{3/2}$, the interactions of the helicity 1/2 components are dominant, and can be well described by the goldstino interactions due to the gravitino-goldstino equivalence theorem [39, 40]. As a consequence of the super-Higgs mechanism, the gravitino mass is related to the SUSY breaking scale and the Planck mass as [41, 42]

$$m_{3/2} = \frac{F}{\sqrt{3} M_{\text{Pl}}}, \quad (2.4)$$

¹The covariant derivative is defined as $D_\mu = \partial_\mu + ig_s T^a A_\mu^a$.

²Note that we follow the FEYNRULES convention for chiral superfields $\Phi(y, \theta) = \phi(y) + \sqrt{2} \theta \cdot \psi(y) - \theta \cdot \theta F(y)$ [38], which fixes the sign of the Lagrangian so as to give a positive contribution to the scalar potential.

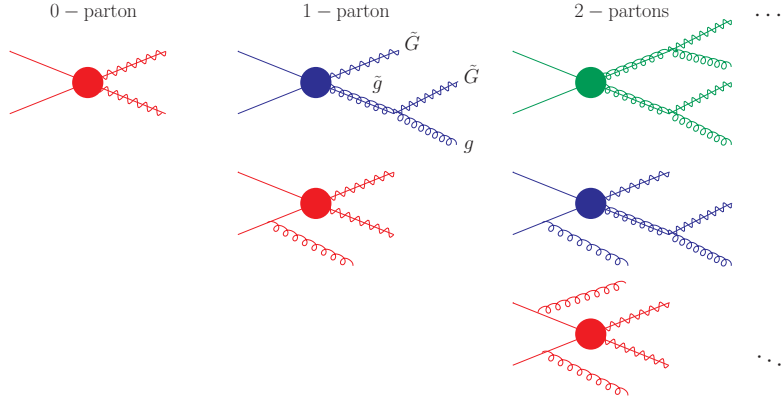


Figure 1. Schematic diagrams for $pp \rightarrow \tilde{G}\tilde{G} + 0, 1, 2$ partons. In the first row the leading gravitino-pair (red), gluino–gravitino (blue) and gluino-pair (green) diagrams are sorted. The diagrams are ordered with the number of additional QCD partons in rows, while with the total parton multiplicity in columns.

where $\overline{M}_{\text{Pl}} \equiv M_{\text{Pl}}/\sqrt{8\pi} \approx 2.4 \times 10^{18}$ GeV is the reduced Planck mass. Therefore, low-scale SUSY breaking scenarios such as GMSB provide a gravitino LSP. In the following, we simply call the goldstino “gravitino”.

2.2 Light gravitino production

Given the model we constructed in the previous section, we now consider light-gravitino production in R -parity conserving scenarios that lead to jet(s) plus missing momentum at the LHC:

$$pp \rightarrow \text{jet}(s) + \cancel{E}_T, \quad (2.5)$$

where the missing momentum is carried by two LSP gravitinos. At the leading order in QCD, the relevant processes are:

1. gravitino-pair production in association with a quark/gluon emission from initial state radiation,
2. gravitino production associated with a squark/gluino with the subsequent decay into a gravitino and a quark/gluon,
3. SUSY QCD pair production with the subsequent decay into gravitino and a quark/gluon.

The processes are schematically represented in fig. 1. The processes in the second column of fig. 1 contribute in an obvious way to the mono-jet signal. However, also the 2-parton final states will contribute either in the exclusive 1-jet analysis because one parton might not give rise to a jet or when the analysis is fully or in part inclusive over other jets. In the current ATLAS and CMS mono-jet analyses [24, 25], for example, a second jet is allowed and hence those events potentially fall into the signal region. For the mono- γ , $-Z$ and $-W$ signals, we simply replace the QCD processes by the EW processes, i.e. replace gluinos by neutralinos and charginos.

We now consider each production channel in more detail.

2.2.1 Gravitino pair production

Direct gravitino-pair production at colliders has been studied only in models where all SUSY particles except for the gravitino are too heavy to be produced on-shell, i.e. in the gravitino EFT limit [8, 9, 21]. One of the aims of this article is to extend the previous studies to take into account the effect of other SUSY particles in spectrum. This has been done recently for mono-photon signals at future linear colliders [43], and we now apply for it to the QCD sector for the LHC.

A pair of gravitinos is produced through both the $q\bar{q}$ and gg initial states,

$$pp(q\bar{q}, gg) \rightarrow \tilde{G}\tilde{G}, \quad (2.6)$$

and can be observed if extra radiation is hard enough to be detected, for instance in the form of one or more jets. The helicity amplitudes for the above $2 \rightarrow 2$ processes were presented in terms of the e^+e^- and $\gamma\gamma$ initial states in [43]. A remarkable feature of this production channel is that the corresponding total cross section scales as the inverse of the gravitino mass to the fourth power,

$$\sigma(\tilde{G}\tilde{G}) \propto 1/m_{3/2}^4. \quad (2.7)$$

Another feature is that the cross section tends to be larger for heavier squarks and gluinos, which are propagating in the t and u channels. For the gg channel, there are diagrams featuring s -channel sgoldstino. These play an important role in the computation of cross sections even when sgoldstinos are too heavy to be produced; see ref. [43] for more details.

As expected from the colourless nature of the gravitinos, an extra parton in the final state mainly comes from initial state radiation and therefore it is naturally suppressed by α_S/p_T^4 . Hence the mono-jet rate from this process strongly depends on the jet minimum p_T (or equivalently from the minimum missing momentum). We will investigate those effects carefully in sec. 3. The $2 \rightarrow 3$ processes

$$pp(q\bar{q}, qg, gg) \rightarrow \tilde{G}\tilde{G}j, \quad (2.8)$$

have been calculated for $q\bar{q}$ and qg initial states in the gravitino EFT limit, yet the gg process was estimated only by the $2 \rightarrow 2$ cross section in the limit of the soft and collinear gluon radiation [21]. In this article, as shown later, we consider all the amplitudes at tree-level without any approximation and calculate the full matrix elements numerically.

2.2.2 Associated gravitino production

Gravitino production in association with a squark or a gluino and the subsequent decay into a gravitino and a quark/gluon,

$$pp \rightarrow \tilde{q}\tilde{G}, \tilde{g}\tilde{G} \rightarrow \tilde{G}\tilde{G}j, \quad (2.9)$$

leads to the $j + \cancel{E}_T$ signal at the leading order (LO), and has been studied in [30–35]. The tree-level ME+PS merging technique has also been applied for this process in [36].

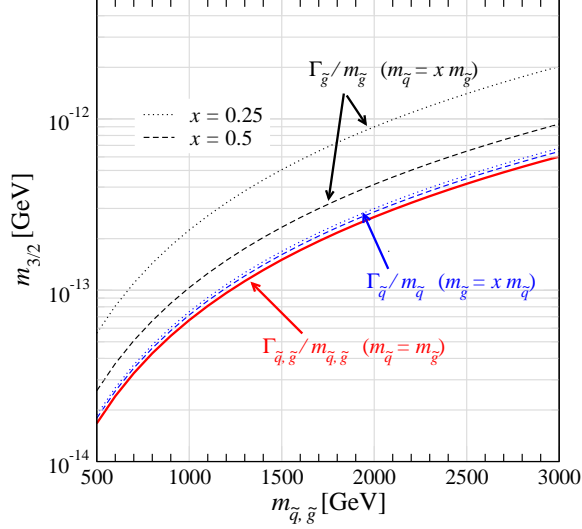


Figure 2. 25% lines of the total width over the mass in the squark (gluino) and gravitino mass plane for $m_{\tilde{q}} = m_{\tilde{g}}$ (red), $m_{\tilde{q}} > m_{\tilde{g}}$ (blue), and $m_{\tilde{q}} < m_{\tilde{g}}$ (black) cases, where the main decay mode is $\tilde{q}(\tilde{g}) \rightarrow q(g) + \tilde{G}$. For the non-degenerate case, we take $m_{\tilde{g}} = \{4, 2, 1/2, 1/4\} \times m_{\tilde{q}}$.

Unlike the gravitino-pair production in eq. (2.7), the cross section is inversely proportional to the square of the gravitino mass,

$$\sigma(\tilde{q}\tilde{G}, \tilde{g}\tilde{G}) \propto 1/m_{3/2}^2, \quad (2.10)$$

and hence the dependence of the gravitino mass is milder than in the gravitino-pair production. Similar to the $\tilde{G}\tilde{G}$ production, heavier squarks and gluinos in the t and u channels enhance the cross sections, while those in the final state suppress the cross sections due to the phase space.

2.2.3 Indirect gravitino production

SUSY QCD pair productions, i.e. squark-pair, gluino-pair and squark–gluino productions, have been systematically studied, motivated by the inclusive SUSY searches as well as in simplified SUSY searches. On the other hand, they have not been considered in the mono-jet analysis since more than one jet in the final state is expected. Especially, when squarks and/or gluinos are the next-to-lightest SUSY particle (NLSP), their decay can provide the di-jet plus missing momentum signal at the LO [44, 45]:

$$pp \rightarrow \tilde{q}\tilde{q}, \tilde{q}\tilde{g}, \tilde{g}\tilde{g} \rightarrow \tilde{G}\tilde{G}jj. \quad (2.11)$$

As mentioned above, in the current mono-jet analyses by ATLAS [24] and CMS [25], events with a second jet have been included as the signal typically contains more jets from QCD radiation. Therefore, depending on cuts, the jets coming from the decay of heavy SUSY particles may contribute to the signal region. We also note that, when the gravitino is very light, the t -channel gravitino exchange enhances the cross sections [30–33].

Before turning to the collider phenomenology part, it may be worth to mention the decay width of the squark and gluino. The partial decay width of a squark (gluino) into a quark (gluon) and a gravitino is given by

$$\Gamma(\tilde{q}(\tilde{g}) \rightarrow q(g) + \tilde{G}) = \frac{m_{\tilde{q}(\tilde{g})}^5}{48\pi \overline{M}_{\text{Pl}}^2 m_{3/2}^2}, \quad (2.12)$$

where the gravitino mass in the phase space is neglected. When the gravitino is very light and/or the squarks and gluinos are heavy, the width of the squark and gluino can be a significant fraction of the mass. At the same time, the gravitino couplings become strong and the perturbative calculations are not reliable. To identify a reasonable SUSY parameter space, in fig. 2 we show $\Gamma/m = 0.25$ lines for $m_{\tilde{q}} = m_{\tilde{g}}$ (red), $m_{\tilde{q}} > m_{\tilde{g}}$ (blue), and $m_{\tilde{q}} < m_{\tilde{g}}$ (black).³ We assume all other SUSY particles are heavier than the squarks and the gluino. For the $m_{\tilde{q}} > m_{\tilde{g}}$ case, the additional $\tilde{q} \rightarrow \tilde{g} + q$ decay channel is opened. For the $m_{\tilde{q}} < m_{\tilde{g}}$ case, on the other hand, the gluino has all possible squark decay modes, and hence its width becomes significantly larger than the squark one, strongly depending on the mass difference. In the following, a benchmark scenario will be identified ($m_{3/2} = 2 \times 10^{-13}$ GeV with $m_{\tilde{q}} = m_{\tilde{g}} = 1$ TeV) where the widths are 28 GeV.

2.3 Event simulation tools

Here, we briefly describe event simulation tools we employ in this article. We follow the strategy presented in ref. [47] to new physics simulations.

Similar to the SUSY QED model of ref. [43], we have implemented the SUSY QCD Lagrangian with a goldstino supermultiplet described in sec. 2.1 into FEYNRULES2 [38], which provides the Feynman rules in terms of the physical component fields and the UFO model file [48, 49] for matrix-element generators such as MADGRAPH5_AMC@NLO [50]. In this work, instead of employing a dedicated implementation of the four-fermion vertices involving more than one Majorana particle [43], we introduce auxiliary heavy particles for the multi-jet simulation. Parton-level events generated by MADGRAPH5_AMC@NLO are passed to PYTHIA6.4 [51] for parton shower and hadronisation, to DELPHES3 [52] for detector simulation, and to MADANALYSIS5 [53] for sample analyses.

3 Mono-jet plus missing momentum

In this section, we first present total and differential cross sections to illustrate how the three gravitino production processes depend on the SUSY mass parameters. Then, we recast the ATLAS mono-jet analysis [24] to constrain the gravitino mass in cases that go beyond the gravitino-EFT scenario.

³The widths are obtained numerically by the decay package MADWIDTH [46].

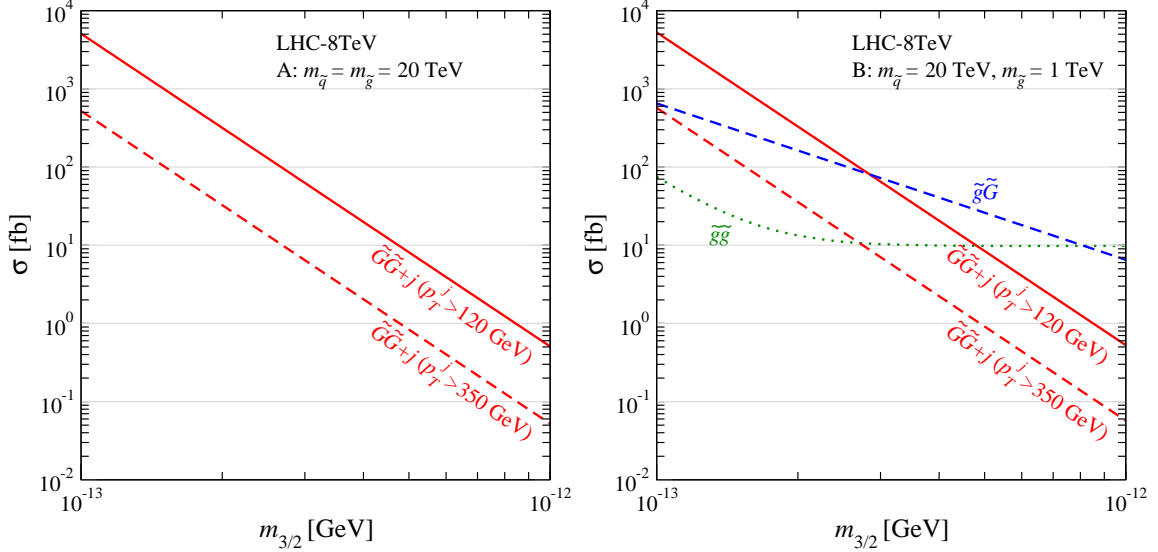


Figure 3. Total cross sections of the gravitino-pair production with a QCD radiation ($\tilde{G}\tilde{G} + j$), the gluino-gravitino associated production ($\tilde{g}\tilde{G}$), and the gluino-pair production ($\tilde{g}\tilde{g}$) at $\sqrt{s} = 8$ TeV as a function of the gravitino mass for case A (left) and B (right). For the gravitino-pair production kinematical cuts $p_T^j > 120/350$ GeV (solid/dashed) and $|\eta^j| < 4.5$ are applied.

In the following, we consider three scenarios where squark and/or gluino masses are $\mathcal{O}(10)$ TeV and $\mathcal{O}(1)$ TeV:

$$A : \quad m_{\tilde{q}} = m_{\tilde{g}} = 20 \text{ TeV} \quad (\text{the gravitino-EFT limit}), \quad (3.1a)$$

$$B : \quad m_{\tilde{q}} = 20 \text{ TeV}, \quad m_{\tilde{g}} = 1 \text{ TeV} \quad (\text{the heavy-squark limit}), \quad (3.1b)$$

$$C : \quad m_{\tilde{q}} = m_{\tilde{g}} = 1 \text{ TeV}, \quad (3.1c)$$

while we keep the sgoldstino masses at 20 TeV. For simplicity, we assume that all the non-colored SUSY particles are heavier than the colored ones, and hence the decay mode of squarks and gluinos is only into gravitinos. Only the gravitino-pair production contributes to the signal for case A, while the $\tilde{g}\tilde{G}$ and $\tilde{g}\tilde{g}$ productions can also give the signal for case B. In case C all the subprocesses can be comparable. We note that the masses $m_{\tilde{q}} = m_{\tilde{g}} = 20$ TeV reproduce the results of the total and differential cross sections in ref. [21], where all the SUSY particles except gravitinos are integrated out, i.e. where the computation has been done in the gravitino-EFT limit.

3.1 Total rates

Figures 3 and 4 (left) show the total cross sections as a function of the gravitino mass for the three scenarios at $\sqrt{s} = 8$ TeV. For the gravitino-pair production plus an extra QCD emission ($\tilde{G}\tilde{G} + j$), we impose a minimal transverse momentum cut for the jet with $p_T^j > 120$ GeV and 350 GeV in the region $|\eta^j| < 4.5$. We employ the CTEQ6L1 PDFs [54] with the factorization and renormalization scales at p_T^j for the gravitino-pair production, $(m_{\tilde{q},\tilde{g}} + m_{3/2})/2 \sim m_{\tilde{q},\tilde{g}}/2$ for the associated gravitino production, and $(m_{\tilde{q},\tilde{g}} + m_{\tilde{q},\tilde{g}})/2 \sim$

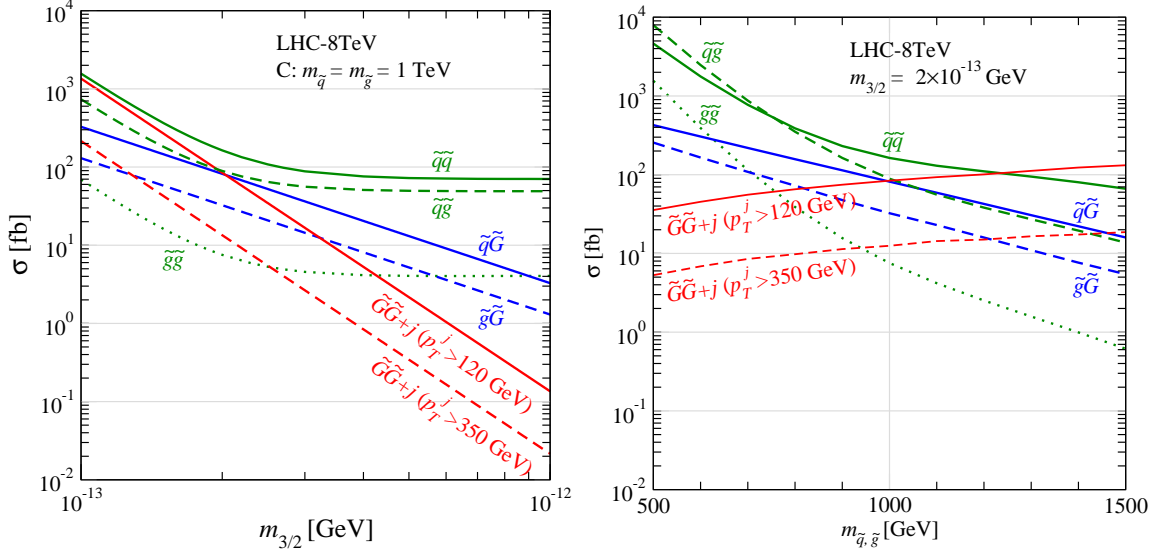


Figure 4. Left: Same as fig. 3, but for case C. Right: Total cross sections as a function of the degenerate squark and gluino masses with the gravitino mass at $m_{3/2} = 2 \times 10^{-13}$ GeV.

$m_{\tilde{q}, \tilde{g}}$ for the SUSY QCD pair production. We note that all our results are the LO predictions although it is well known that higher-order QCD corrections are large. For example, the K factor of the gluino-pair production is about three for $m_{\tilde{g}} \sim 1$ TeV at the 8-TeV LHC [55, 56], while the higher-order calculations have not yet been done for the gravitino-pair production and the associated gravitino production. Our analyses can be redone with different overall normalizations and yet the main features will not change.

One can clearly see the $m_{3/2}^{-4}$ and $m_{3/2}^{-2}$ dependence for the $\tilde{G}\tilde{G}(+j)$ and $\tilde{q}\tilde{G}/\tilde{g}\tilde{G}$ processes, respectively, as discussed in sec. 2.2. For the SUSY QCD pair productions, $\tilde{q}\tilde{q}/\tilde{q}\tilde{g}/\tilde{g}\tilde{g}$, the contribution of the t -channel gravitino exchange can be visible if the gravitino is lighter than about 3×10^{-13} GeV.

We also show the total rates as a function of the degenerate squark and gluino masses with the fixed gravitino mass at 2×10^{-13} GeV in fig. 4 (right). For the gravitino-pair production, the cross section increases as the squarks and gluinos become heavier. On the other hand, the cross sections for the associated production and the SUSY QCD pair production decreases due to the phase space suppression.

As can be seen in figs. 3 and 4, each contribution to the total rates strongly depends on the SUSY mass parameters, and the different contributions can be comparable for certain parameters. However, the resulting signature can be still distinctive among the subprocesses as shown below.

3.2 Differential distributions

We now consider differential distributions for the direct gravitino-pair production in detail. This is the first presented result that goes beyond the gravitino EFT limit. Figure 5 shows normalized missing transverse momentum distributions for the three benchmark scenarios in (3.1). Here parton-shower and detector effects are included, and the detector

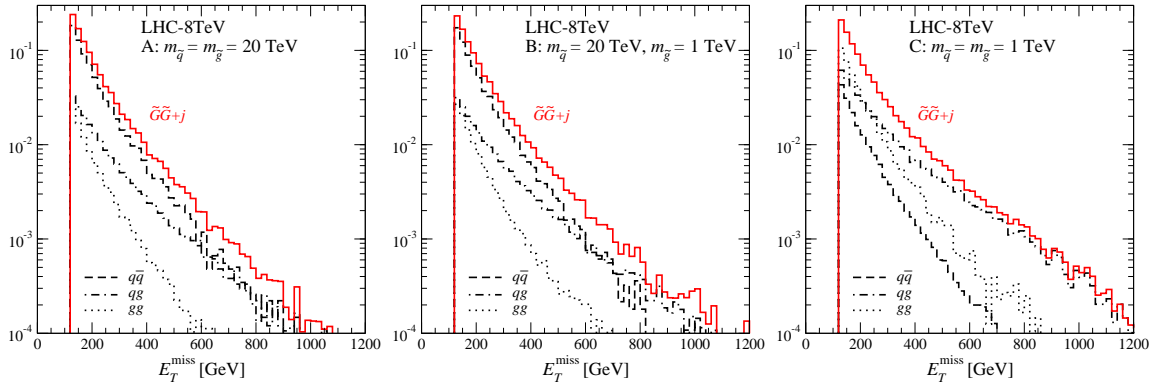


Figure 5. Normalized missing transverse energy distributions of the direct gravitino-pair production with an extra radiation for the three benchmarks in (3.1) at the LHC-8TeV. Parton-shower and detector effects are included for the event generation and a cut $\cancel{E}_T > 120$ GeV is imposed. The contributions from different initial states are also shown.

acceptance cuts $p_T^j > 20$ GeV and $|\eta^j| < 4.5$ as well as the missing transverse momentum cut $\cancel{E}_T > 120$ GeV are applied. Jets are reconstructed employing the anti- k_T algorithm [57] with a radius parameter of 0.4. Depending on the mass of the t -channel exchanged squarks and gluinos, the contributions from different initial states can be of different relevance. Moreover, the energy spectra from $q\bar{q}$ and gg are similar, while that from qg is harder than the others.

Figure 6 presents several kinematical distributions of all the production channels for case C as well as the SM $Z + j$ background. We stress that the purpose of including the $Z + j$ background is illustrative on the one hand and to provide a “normalisation” point for experimentalists. Needless to say, many other important sources of backgrounds need to be included for a complete analysis, such as those coming from $W + \text{jets}$ or just (mis-measured) jets. Most of them, however, can only be meaningfully estimated in presence of a detailed detector simulation and data validation.

We see that the SUSY signals are harder than the SM background, even for the gravitino-pair production. This is mainly due to the $2 \rightarrow 3$ kinematics of the signal, whereas the background essentially has the $2 \rightarrow 2$ kinematics. Besides the background, $\tilde{G}\tilde{G}(+j)$ has the softest spectra, while $\tilde{q}\tilde{q}/\tilde{q}\tilde{g}/\tilde{g}\tilde{g}$ lead the hardest. The differences in the p_T spectrum of the second-leading jet are rather significant. The second jet mostly comes from the squark or gluino decay for the SUSY QCD pair production, while mainly from QCD radiation in the gravitino-pair and associated productions. We note that the shapes for the available subprocesses are very similar among the three scenarios in (3.1), while the rates are different as seen in the previous subsection.

3.3 Recasting LHC mono-jet analyses

ATLAS and CMS have reported a search for new physics in mono-jet plus missing transverse momentum final states. The null results are translated into limits on a gauge-mediated SUSY, large extra dimension and dark matter models in ATLAS [24] and on dark matter, large extra dimension and unparticle models in CMS [25]. As mentioned in the introduc-

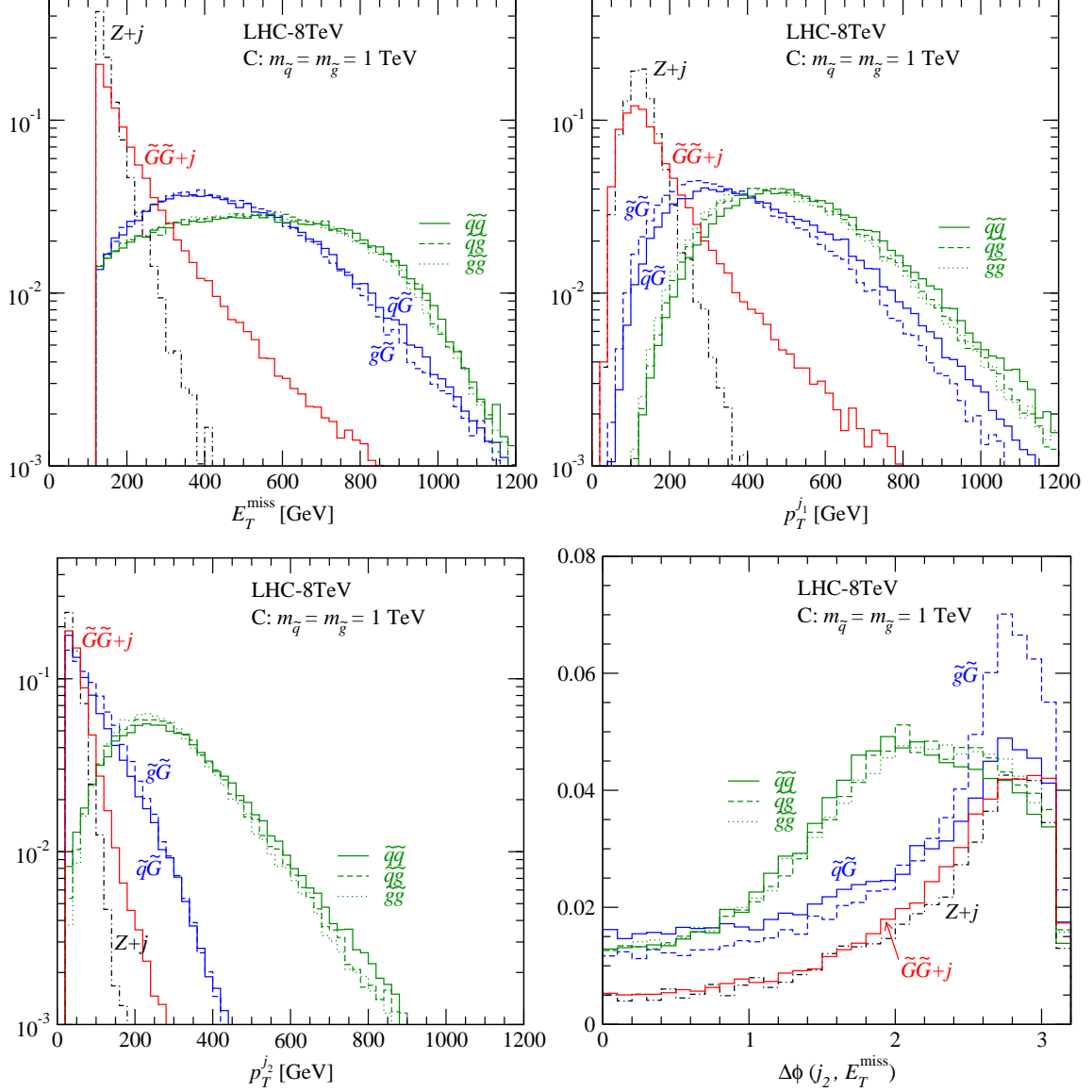


Figure 6. Normalized distributions for each signal subprocess with $m_{3/2} = 2 \times 10^{-13}$ GeV and $m_{\tilde{q}, \tilde{g}} = 1$ TeV at the LHC-8TeV. Parton-shower and detector effects are included for the event generation, and a cut $\cancel{E}_T > 120$ GeV is imposed. As a reference, the $Z(\rightarrow \nu\bar{\nu}) + j$ background is also shown.

tion, in the ATLAS analysis, a light gravitino scenario has been studied, but only the squark-gravitino and gluino-gravitino associated productions. In this section, taking into account all the possible gravitino production processes described above, we recast the ATLAS 8-TeV mono-jet analysis with 10.5 fb^{-1} data [24] to constrain the gravitino mass for different squark and gluino masses.

	A	B			C						bkg
	$\tilde{G}\tilde{G}$	$\tilde{G}\tilde{G}$	$\tilde{g}\tilde{G}$	$\tilde{g}\tilde{g}$	$\tilde{G}\tilde{G}$	$\tilde{q}\tilde{G}$	$\tilde{g}\tilde{G}$	$\tilde{q}\tilde{q}$	$\tilde{q}\tilde{g}$	$\tilde{g}\tilde{g}$	$Z + j$
$\cancel{E}_T > 120$ GeV	5257	5433	1770	140	1400	878	353	1716	938	79	329893
+ $p_T^{j_1} > 120$ GeV	3164	3291	1672	139	800	836	336	1698	929	79	163270
+ at most 2 jets	2776	2869	1108	15	614	550	180	589	138	6	152532
SR1 + $\Delta\phi(j_2, \cancel{E}_T) > 0.5$	2690	2778	1061	14	583	508	170	551	128	5	146548
SR1' + $p_T^{j_2} < 150$ GeV	2652	2736	959	3	564	455	152	88	23	1	145954
SR1 + $\cancel{E}_T > 250$ GeV	869	914	956	13	229	454	153	497	116	5	12604
SR2 + $p_T^{j_1} > 250$ GeV	614	654	863	12	170	424	138	487	114	5	7554
SR2' + $p_T^{j_2} < 150$ GeV	591	628	778	2	157	379	123	75	21	1	7512
SR2 + $\cancel{E}_T > 350$ GeV	340	369	762	11	109	361	120	432	102	4	2037
SR3 + $p_T^{j_1} > 350$ GeV	254	281	660	10	86	323	103	403	94	4	1358
SR3' + $p_T^{j_2} < 150$ GeV	243	268	604	2	79	291	93	61	17	1	1358

Table 1. SUSY signal predictions of the three scenarios in (3.1) with $m_{3/2} = 2 \times 10^{-13}$ GeV for the number of events passing each step of the selection requirements in (3.2) and (3.3), expected for an integrated luminosity of 10.5 fb^{-1} at the LHC-8TeV. $Z(\rightarrow \nu\bar{\nu}) + j$ background is also shown as a reference.

3.3.1 Selection cuts

The event selection of the ATLAS analysis [24] is

1. $\cancel{E}_T > 120$ GeV,
 2. leading jet with $p_T^{j_1} > 120$ GeV and $|\eta^{j_1}| < 2.0$,
 3. at most two jets with $p_T^j > 30$ GeV and $|\eta^j| < 4.5$,
 4. $\Delta\phi(j_2, \cancel{E}_T) > 0.5$.
- (3.2)

The third requirement allows the second-leading jet (j_2) since signal events typically contain jets from initial state radiation, while the last one reduces the QCD background where the large \cancel{E}_T originates from the mis-measurement of $p_T^{j_2}$. On top of the above requirements, similarly to the ATLAS analysis, we define three signal regions (SRs) with different \cancel{E}_T and $p_T^{j_1}$ thresholds as⁴

$$\begin{aligned}
\text{SR1} : \quad & \cancel{E}_T, p_T^{j_1} > 120 \text{ GeV}, \\
\text{SR2} : \quad & \cancel{E}_T, p_T^{j_1} > 250 \text{ GeV}, \\
\text{SR3} : \quad & \cancel{E}_T, p_T^{j_1} > 350 \text{ GeV}.
\end{aligned}
\tag{3.3}$$

In table 1 we present SUSY signal predictions for the number of events passing each step of the above selection requirements. As in fig. 6, we generate events for each subprocess including parton-shower and detector effects. In addition to the three SUSY benchmark scenarios in (3.1) with the gravitino mass at 2×10^{-13} GeV, we show the $Z(\rightarrow \nu\bar{\nu}) + j$ background prediction, which is the dominant background, as a reference; see table 2 in the ATLAS analysis [24] for more details on the background estimation including other channels.

⁴SR2 in the ATLAS analysis is with the 220 GeV cut [24]. On the other hand, our SR2 is similar to the one of the signal regions in the CMS analysis [25].

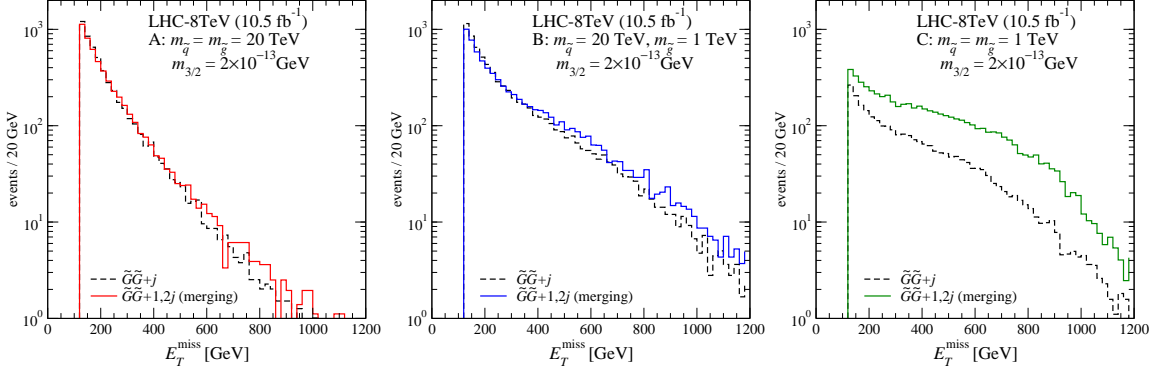


Figure 7. Missing transverse energy distributions for the three scenarios in (3.1) with $m_{3/2} = 2 \times 10^{-13}$ GeV, where the inclusive samples of the $\tilde{G}\tilde{G}+1$ parton in the matrix element (dashed) are compared with the merged samples containing an extra parton (solid). Only the cut $\cancel{E}_T > 120$ GeV is applied.

At the LO parton level, $\cancel{E}_T = p_T^{j1}$ for the $\tilde{G}\tilde{G}(+j)$ and $\tilde{q}\tilde{G}/\tilde{g}\tilde{G}$ productions. After the parton shower, the relation does not hold any more, and the effect of the radiation is quite large for the gravitino pair production. As expected, the third selection cut in (3.2) does not affect so much for $\tilde{G}\tilde{G}(+j)$ and $\tilde{q}\tilde{G}/\tilde{g}\tilde{G}$, while significantly reduces the SUSY QCD pair contributions although for case C the contribution is still substantial and even dominant in SR3. We remind the reader that SUSY QCD pair production is insensitive to the gravitino mass if the gravitino is heavier than 3×10^{-13} GeV, and hence these contributions have to be considered as background to constrain the gravitino mass. To reduce this SUSY QCD background, on top of the above signal selection cuts, we impose a maximal p_T cut on the second-leading jet in each SR as

$$p_T^{j2} < 150 \text{ GeV}, \quad (3.4)$$

denoted as SR1', SR2' and SR3'. As can be also seen in the p_T^{j2} distribution in fig. 6, this cut removes the large part of the events coming from $\tilde{q}\tilde{q}$, $\tilde{q}\tilde{g}$ and $\tilde{g}\tilde{g}$.

3.3.2 Merging matrix elements with parton showers

So far, in order to identify characteristics and differences among them we have treated each gravitino-production subprocess independently. Now, to constrain the SUSY mass parameters, we generate inclusive signal samples by using the ME+PS merging procedure. In practice, following ref. [36], we make use of the shower- k_T scheme [58], and generate signal events with parton multiplicity from one to two, $pp \rightarrow \tilde{G}\tilde{G}+1, 2$ partons, and merging separation parameters $Q_{\text{cut}} = 60$ GeV and $p_{T_{\text{min}}} = 50$ GeV. We checked carefully that the variation of Q_{cut} did not change the distributions after the minimal missing transverse energy cut $\cancel{E}_T > 120$ GeV. The factorization and renormalization scales are set to the scalar sum of the p_T of all the partons in the final state. We note that the employment of the ME+PS merging procedure allows us to treat different contributing processes, i.e. gravitino-pair, associated gravitino and SUSY QCD pair productions (see also fig. 1), within one event simulation and without double counting. We also note that the interference

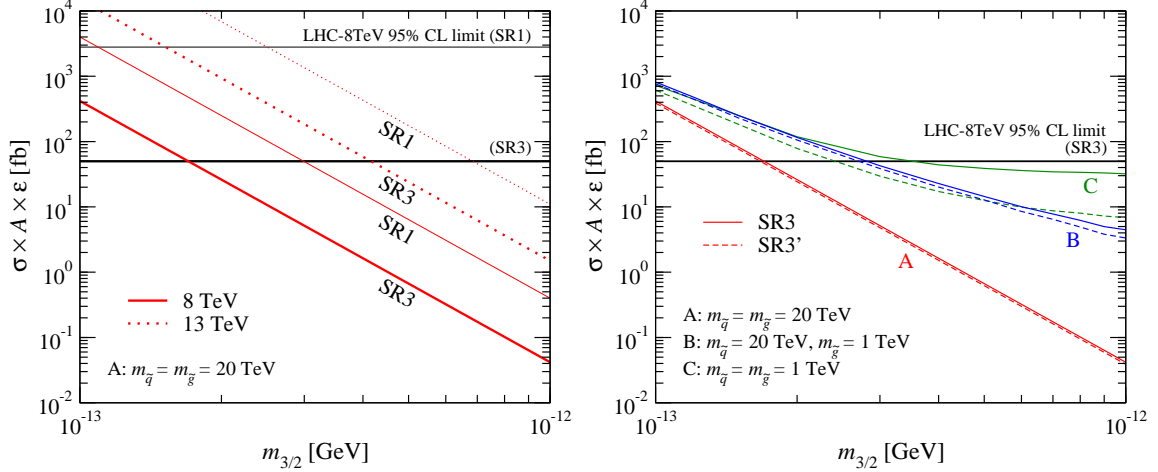


Figure 8. Left: Visible cross sections of the mono-jet signal for case A at $\sqrt{s} = 8$ TeV (solid) and 13 TeV (dotted) as a function of the gravitino mass, where SR1 and SR3 are shown. The predictions are compared with the model-independent 95% confidence level (CL) upper limits by the ATLAS analysis [24]. Right: Same as the left panel, but for all the three scenarios in SR3 (solid) and SR3' (dashed) at $\sqrt{s} = 8$ TeV.

among the different production processes is very small since the width of the on-shell squarks and gluinos is small with our parameter choice.

To see the effect of an extra parton in the matrix element, in fig. 7 we compare the inclusive samples of the $\tilde{G}\tilde{G} + 1$ parton in the matrix element with the merged samples of $pp \rightarrow \tilde{G}\tilde{G} + 1, 2$ partons. For case A, where only the gravitino-pair production contributes, we find a slightly harder spectrum in the high \cancel{E}_T region for the merged sample due to the second parton in the matrix element. For case B, as seen in table 1, besides $\tilde{G}\tilde{G}$, the $\tilde{g}\tilde{G}$ production contributes significantly, leading to a much harder spectrum than in case A. Again, a harder spectrum for the merged sample is observed as expected. For case C, with the minimal selection cut $\cancel{E}_T > 120$ GeV, the SUSY QCD pair productions, especially $\tilde{q}\tilde{q}$ and $\tilde{q}\tilde{g}$, are dominant, which do not exist in the $\tilde{G}\tilde{G} + 1$ parton sample. Therefore, the distributions are completely different without and with an extra parton in the matrix-element level.

3.3.3 Limit on the gravitino mass

By using the inclusive ME+PS merged samples, we can now recast the ATLAS-8TeV mono-jet analysis with 10.5 fb^{-1} data set [24]. ATLAS reported a model-independent 95% confidence level (CL) upper limit on the visible cross section, defined as the production cross section times kinematical acceptance times detection efficiency ($\sigma \times A \times \epsilon$). The values are $2.8 \times 10^3 \text{ fb}$ and 50 fb for SR1 and SR3 selections, respectively.

Figure 8 (left) presents the visible cross sections for case A at $\sqrt{s} = 8$ and 13 TeV as a function of the gravitino mass. The horizontal lines show the ATLAS 95% CL limits. In SR1 the SM background is huge, and hence only the very light gravitino case can be constrained. The constraint in SR3 is slightly better than in SR1, and the gravitino mass

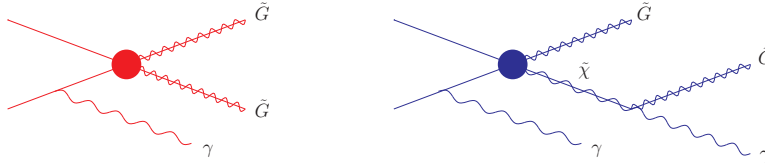


Figure 9. Schematic diagrams for $pp \rightarrow \tilde{G}\tilde{G} + \gamma$, where gravitino-pair production with a photon emission (left) and neutralino–gravitino associated production (right) contribute.

below about 1.7×10^{-13} GeV are excluded at 95% CL in the gravitino EFT. This limit is one order of magnitude stronger than the limits at the LEP and Tevatron [10]. According to the relation in (2.4), the above limit corresponds to the SUSY breaking scale of about 850 GeV. The coming LHC Run-II with $\sqrt{s} = 13$ TeV is expected to explore heavier gravitinos up to $\mathcal{O}(10^{-12})$ GeV, i.e. a few TeV of the SUSY breaking scale.

In fig. 8 (right), the visible cross sections in SR3 at $\sqrt{s} = 8$ TeV are shown for case A, B and C. Roughly speaking, case A and B follow $m_{3/2}^{-4}$ and $m_{3/2}^{-2}$, respectively, as expected. For case C, on the other hand, no sensitivity of the cross section to the gravitino mass is observed when the gravitino mass is heavier than about 3×10^{-13} GeV. However, by imposing an additional cut on the second-leading jet in (3.4), the sensitivity to the gravitino mass recovers even for heavier gravitinos since the SUSY QCD pair productions are strongly suppressed. The maximal p_T^j cut hardly affects the signals for case A and B.

4 Mono-photon, $-Z$, or $-W$ plus missing momentum

In an analogous way to the mono-jet signal discussed in the previous section, superlight gravitino scenarios can provide mono- γ , $-Z$, or $-W$ (mono-EW boson) plus missing momentum signature via

1. gravitino-pair production with a γ , Z , or W emission,
2. gravitino production associated with a neutralino/chargino with the subsequent decay into a γ , Z/W and a gravitino.

The schematic diagrams are shown in fig. 9. Unlike the $j + \cancel{E}_T$ signal, only the $q\bar{q}$ initial state can contribute to the mono-EW boson+ \cancel{E}_T signal. In this section, for simplicity, we consider the heavy neutralino/chargino limit, where only the gravitino-pair production contributes.⁵

So far, new physics searches in mono- γ , $-Z$ and $-W$ signals at the LHC have been done independently, but the combined analysis may be very interesting because there is a possibility to determine left–right handedness of the new physics interactions. Instead of studying the gravitino-mass constraint in each search channel, fig. 10 shows the ratio of the p_T distributions of the massive gauge boson to that of the photon for $pp \rightarrow \tilde{G}\tilde{G}V$ ($V = \gamma, Z, W$) at $\sqrt{s} = 8$ TeV with $m_{3/2} = 1 \times 10^{-13}$ GeV. There are t -channel squark

⁵The mono-photon signal of $\tilde{\chi}_1^0 \tilde{G}$ production via the Higgs decay at the LHC was studied in [59].

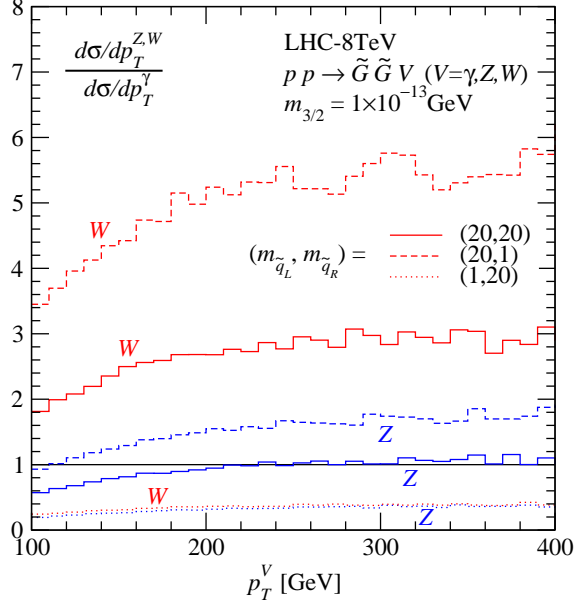


Figure 10. Ratio of the transverse momentum distributions of the Z or W boson to that of the photon for $pp \rightarrow \tilde{G}\tilde{G}V$ ($V = \gamma, Z, W$) at $\sqrt{s} = 8$ TeV with $m_{3/2} = 1 \times 10^{-13}$ GeV. Three scenarios for different left- and right-handed squark masses are considered.

exchange diagrams, and for illustration we take three left- and right-handed squark mass scenarios:

$$(m_{\tilde{q}_L}, m_{\tilde{q}_R}) = \{(20, 20), (20, 1), (1, 20)\} \text{ TeV}. \quad (4.1)$$

The effect of the mass of the gauge boson can be seen as suppression and enhancement in the low and high p_T region, respectively. Interestingly, the ratios are very sensitive to the mass difference between \tilde{q}_L and \tilde{q}_R , especially for the W boson, which only couples to the left-handed squarks.

Finally, we recast the LHC-8TeV mono-photon analyses [22, 23], where non-SUSY models were studied, to constrain the gravitino mass. For event selection, we follow the $\gamma + \cancel{E}_T$ analysis by ATLAS [23]. Events in the signal region are required to have the missing transverse energy $\cancel{E}_T > 150$ GeV and a photon with $p_T > 125$ GeV and $|\eta| < 1.37$. The photon and the missing momentum vector are also required to be well separated as $\Delta\phi(\gamma, \cancel{E}_T) > 0.4$. Possible jets produced by ISR are defined by the anti- k_T algorithm [60] with a radius parameter of 0.4 and are required to be in the region $|\eta| < 4.5$ with $p_T > 30$ GeV. While events with more than one jet are rejected, events with one jet with $\Delta R(\gamma, j) > 0.2$ and $\Delta\phi(\cancel{E}_T, j) > 0.4$ are kept for the signal with ISR, where $\Delta R = \sqrt{(\Delta\eta)^2 + (\Delta\phi)^2}$.

Figure 11 shows the p_T distributions of the photon for $pp \rightarrow \tilde{G}\tilde{G}\gamma$ at $\sqrt{s} = 8$ TeV, where all the above selection cuts are applied except the p_T^γ and \cancel{E}_T cuts. The gravitino mass is fixed at 1×10^{-13} GeV, while the masses of squarks are taken at 1, 2, and 20 TeV. As discussed in the mono-jet signal, the cross section for the gravitino-pair production becomes larger as the t -channel squark masses increase. In analogy with the mono-jet

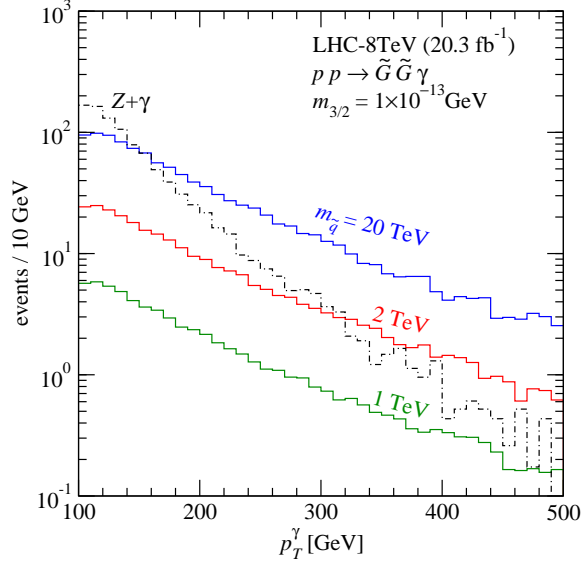


Figure 11. Transverse momentum distributions of the photon for $pp \rightarrow \tilde{G}\tilde{G}\gamma$ at $\sqrt{s} = 8$ TeV with $m_{3/2} = 1 \times 10^{-13}$ GeV for three squark masses. All selection cuts described in the text are applied except the p_T^γ and \cancel{E}_T cuts. The $Z(\rightarrow \nu\bar{\nu}) + \gamma$ background is also shown as a reference.

case, the SUSY signal is harder than the SM background mainly due to the kinematics. We note again that the signal rate strongly depends on the gravitino mass as $m_{3/2}^{-4}$ and also on the kinematical cuts.

The ATLAS $\gamma + \cancel{E}_T$ study with 20.3 fb^{-1} of collisions at $\sqrt{s} = 8$ TeV reported a model-independent 95% CL upper limit on the fiducial cross section, $\sigma \times A$. The value is 5.3 fb [23]. Figure 12 presents the visible cross sections for $pp \rightarrow \gamma\tilde{G}\tilde{G}$ at $\sqrt{s} = 8$ and 13 TeV as a function of the gravitino mass for three different squark masses. The horizontal line shows the ATLAS 95% CL limit, where we take a conservative estimate for the fiducial reconstruction efficiency $\varepsilon = 0.7$ [23].

Gravitino masses below about 1.7×10^{-13} GeV are excluded at 95% CL for the heavy SUSY mass limit, which is translated to the lower bound on the SUSY breaking scale of about 850 GeV, similar to the mono-jet limit. For lighter squark masses the limits are lower, for example, $m_{3/2} \sim 8.4 \times 10^{-14}$ GeV, i.e. $\sqrt{F} \sim 600$ GeV for 1-TeV squarks. These results significantly improve previous ones at LEP and the Tevatron, and are comparable with the recent ATLAS 8-TeV mono-jet analysis [24].⁶ The coming LHC Run-II with $\sqrt{s} = 13$ TeV is expected to explore heavier gravitinos up to $\mathcal{O}(10^{-12})$ GeV, i.e. a few TeV of the SUSY breaking scale. We note that we assumed the heavy neutralino limit in this section. However, if the neutralino is light enough and promptly decays, production of the on-shell neutralino can give rise to characteristic harder photons. This leads to different production rate as well as $A \times \varepsilon$, and hence the limits can be modified. The discussions for the mono-jet study in the previous section can be applied for the mono-photon case by the replacement of gluino/gluon to neutralino/photon for the $q\bar{q}$ initial state.

⁶In the ATLAS study, only associated gravitino production with a gluino or a squark was considered.

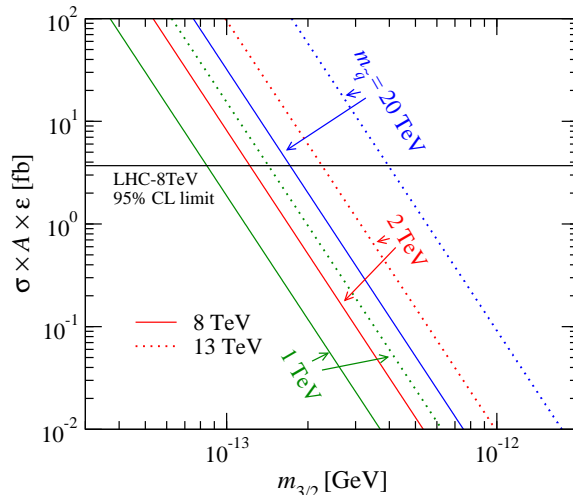


Figure 12. Visible cross sections of the mono-photon signal at $\sqrt{s} = 8$ TeV (solid) and 13 TeV (dotted) as a function of the gravitino mass for different squark masses. The predictions are compared with the model-independent 95% confidence level (CL) upper limit by the ATLAS analysis [23].

5 Summary

The mono-jet plus missing momentum signal at the LHC is a promising final state where to look for new physics. In this work we investigated the possibility of observing a SUSY signal via a very light gravitino. Gravitino-pair production with extra radiation and associated gravitino production with a squark or a gluino contribute both to mono-jet signals. Moreover, in the current ATLAS and CMS mono-jet analyses, squark and gluino pair production may contribute to the signal region. We have carefully investigated the impact of consistently including all three production channels. We have constructed a SUSY QCD model, lifting previous limitations of gravitino-EFT models. We have implemented it in the FEYNRULES and MADGRAPH5_AMC@NLO simulation framework paying special attention to needed Majorana four-fermion interactions.

We discussed the parameter dependence of the signal rate in detail and showed that the relative importance of the three contributing subprocesses varies with the gravitino and SUSY particle masses. We also studied the differential distributions to get better understanding of the expected shape for different parameters.

To constrain the gravitino and other SUSY masses we have recast the LHC-8TeV mono-jet analyses by the ATLAS and CMS collaborations. Using matrix-element/parton-shower merged samples, we have been able to treat all three contributing subprocesses within one event simulation and without double counting. Re-interpreting the reported model-independent 95% CL upper limit on the visible cross section, we found that a gravitino mass below about 1.7×10^{-13} GeV is excluded in the limit where all SUSY particles except the gravitino are very heavy. We showed that this limit changes when allowing squarks and gluinos to be relatively light. To get a better sensitivity to the gravitino mass, we suggest an additional cut in the analysis which suppresses contributions from SUSY QCD pair production. We have also discussed prospects for the LHC Run-II, which is expected

to explore gravitino masses up to $\mathcal{O}(10^{-12})$ GeV.

Finally, we also considered production of EW particles and investigated the mono-photon, $-Z$ and $-W$ plus missing momentum signals. We have performed a detailed analysis for gravitino-pair production, showing that the ratios of the different vector bosons in the final state might reveal information about left- and right-handed couplings. We have reinterpreted the mono-photon analysis at $\sqrt{s} = 8$ TeV, and found a similar limit as in the mono-jet analysis in the case where all SUSY particles except the gravitino are very heavy. For lighter squark masses, the limits are lower. We have concluded by presenting the outlook for the LHC Run-II.

Acknowledgments

This work has been performed in the framework of the ERC grant 291377 “LHCtheory: Theoretical predictions and analyses of LHC physics: advancing the precision frontier” and of the FP7 Marie Curie Initial Training Network MCnetITN (PITN-GA-2012-315877). It is also supported in part by the Belgian Federal Science Policy Office through the Interuniversity Attraction Pole P7/37. The work of AM and FM is supported by the IISN “MadGraph” convention 4.4511.10 and the IISN “Fundamental interactions” convention 4.4517.08. KM and BO are supported in part by the Strategic Research Program “High Energy Physics” and the Research Council of the Vrije Universiteit Brussel.

References

- [1] A. DiFranzo, K. I. Nagao, A. Rajaraman, and T. M. Tait, *Simplified Models for Dark Matter Interacting with Quarks*, *JHEP* **1311** (2013) 014, [[arXiv:1308.2679](#)].
- [2] J. Abdallah, A. Ashkenazi, A. Boveia, G. Busoni, A. De Simone, et al., *Simplified models for dark matter and missing energy searches at the LHC*, [arXiv:1409.2893](#).
- [3] S. Malik, C. McCabe, H. Araujo, A. Belyaev, C. Boehm, et al., *Interplay and characterization of dark matter searches at colliders and in direct detection experiments*, [arXiv:1409.4075](#).
- [4] **OPAL** Collaboration, G. Abbiendi et al., *Photonic events with missing energy in e^+e^- collisions at $\sqrt{s} = 189$ GeV*, *Eur.Phys.J.* **C18** (2000) 253–272, [[hep-ex/0005002](#)].
- [5] **ALEPH** Collaboration, A. Heister et al., *Single photon and multiphoton production in e^+e^- collisions at \sqrt{s} up to 209 GeV*, *Eur.Phys.J.* **C28** (2003) 1–13.
- [6] **L3** Collaboration, P. Achard et al., *Single photon and multiphoton events with missing energy in e^+e^- collisions at LEP*, *Phys.Lett.* **B587** (2004) 16–32, [[hep-ex/0402002](#)].
- [7] **DELPHI** Collaboration, J. Abdallah et al., *Photon events with missing energy in e^+e^- collisions at $\sqrt{s} = 130$ GeV to 209 GeV*, *Eur.Phys.J.* **C38** (2005) 395–411, [[hep-ex/0406019](#)].
- [8] O. Nachtmann, A. Reiter, and M. Wirbel, *Single jet and single photon production in proton - anti-proton collisions and e^+e^- annihilation in a supersymmetric model*, *Z.Phys.* **C27** (1985) 577.
- [9] A. Brignole, F. Feruglio, and F. Zwirner, *Signals of a superlight gravitino at e^+e^- colliders when the other superparticles are heavy*, *Nucl.Phys.* **B516** (1998) 13–28, [[hep-ph/9711516](#)].

- [10] **Particle Data Group** Collaboration, K. Olive et al., *Review of Particle Physics*, *Chin.Phys.* **C38** (2014) 090001.
- [11] P. Fayet, *Lower Limit on the Mass of a Light Gravitino from e^+e^- Annihilation Experiments*, *Phys.Lett.* **B175** (1986) 471.
- [12] D. A. Dicus, S. Nandi, and J. Woodside, *A New source of single photons from Z^0 decay*, *Phys.Lett.* **B258** (1991) 231–235.
- [13] J. L. Lopez, D. V. Nanopoulos, and A. Zichichi, *Supersymmetric photonic signals at LEP*, *Phys.Rev.Lett.* **77** (1996) 5168–5171, [[hep-ph/9609524](#)].
- [14] J. L. Lopez, D. V. Nanopoulos, and A. Zichichi, *Single photon signals at LEP in supersymmetric models with a light gravitino*, *Phys.Rev.* **D55** (1997) 5813–5825, [[hep-ph/9611437](#)].
- [15] S. Baek, S. C. Park, and J.-h. Song, *Kaluza-Klein gravitino production with a single photon at e^+e^- colliders*, *Phys.Rev.* **D66** (2002) 056004, [[hep-ph/0206008](#)].
- [16] K. Mawatari, B. Oehl, and Y. Takaesu, *Associated production of light gravitinos in e^+e^- and $e^-\gamma$ collisions*, *Eur.Phys.J.* **C71** (2011) 1783, [[arXiv:1106.5592](#)].
- [17] **CDF** Collaboration, T. Affolder et al., *Limits on gravitino production and new processes with large missing transverse energy in $p\bar{p}$ collisions at $\sqrt{s} = 1.8$ TeV*, *Phys.Rev.Lett.* **85** (2000) 1378–1383, [[hep-ex/0003026](#)].
- [18] **CDF** Collaboration, D. Acosta et al., *Limits on extra dimensions and new particle production in the exclusive photon and missing energy signature in $p\bar{p}$ collisions at $\sqrt{s} = 1.8$ TeV*, *Phys.Rev.Lett.* **89** (2002) 281801, [[hep-ex/0205057](#)].
- [19] **D0** Collaboration, V. Abazov et al., *Search for large extra dimensions via single photon plus missing energy final states at $\sqrt{s} = 1.96$ TeV*, *Phys.Rev.Lett.* **101** (2008) 011601, [[arXiv:0803.2137](#)].
- [20] **CDF** Collaboration, T. Aaltonen et al., *Search for large extra dimensions in final states containing one photon or jet and large missing transverse energy produced in $p\bar{p}$ collisions at $\sqrt{s} = 1.96$ TeV*, *Phys.Rev.Lett.* **101** (2008) 181602, [[arXiv:0807.3132](#)].
- [21] A. Brignole, F. Feruglio, M. L. Mangano, and F. Zwirner, *Signals of a superlight gravitino at hadron colliders when the other superparticles are heavy*, *Nucl.Phys.* **B526** (1998) 136–152, [[hep-ph/9801329](#)].
- [22] **CMS** Collaboration, V. Khachatryan et al., *Search for new phenomena in monophoton final states in proton-proton collisions at $\sqrt{s} = 8$ TeV*, [[arXiv:1410.8812](#)].
- [23] **ATLAS** Collaboration, G. Aad et al., *Search for new phenomena in events with a photon and missing transverse momentum in pp collisions at $\sqrt{s} = 8$ TeV with the ATLAS detector*, *Phys.Rev.* **D91** (2015) 012008, [[arXiv:1411.1559](#)].
- [24] **ATLAS** Collaboration, *Search for new phenomena in monojet plus missing transverse momentum final states using 10 fb^{-1} of pp collisions at $\sqrt{s} = 8$ TeV with the ATLAS detector at the LHC*, *ATLAS-CONF-2012-147* (2012).
- [25] **CMS** Collaboration, V. Khachatryan et al., *Search for dark matter, extra dimensions, and unparticles in monojet events in proton-proton collisions at $\sqrt{s} = 8$ TeV*, [[arXiv:1408.3583](#)].
- [26] **ATLAS** Collaboration, G. Aad et al., *Search for dark matter in events with a Z boson and*

- missing transverse momentum in pp collisions at $\sqrt{s}=8$ TeV with the ATLAS detector*, *Phys.Rev.* **D90** (2014) 012004, [[arXiv:1404.0051](#)].
- [27] **ATLAS** Collaboration, G. Aad et al., *Search for new particles in events with one lepton and missing transverse momentum in pp collisions at $\sqrt{s} = 8$ TeV with the ATLAS detector*, *JHEP* **1409** (2014) 037, [[arXiv:1407.7494](#)].
- [28] **CMS** Collaboration, V. Khachatryan et al., *Search for physics beyond the standard model in final states with a lepton and missing transverse energy in proton-proton collisions at $\sqrt{s} = 8$ TeV*, [arXiv:1408.2745](#).
- [29] **CMS** Collaboration, V. Khachatryan et al., *Search for monotop signatures in proton-proton collisions at $\sqrt{s} = 8$ TeV*, [arXiv:1410.1149](#).
- [30] D. Dicus, S. Nandi, and J. Woodside, *Collider signals of a superlight gravitino*, *Phys.Rev.* **D41** (1990) 2347.
- [31] M. Drees and J. Woodside, *Signals for a superlight gravitino at the LHC*, *IS-J-4137*, *C90-10-04* (1990).
- [32] D. A. Dicus and S. Nandi, *New collider bound on light gravitino mass*, *Phys.Rev.* **D56** (1997) 4166–4169, [[hep-ph/9611312](#)].
- [33] J. Kim, J. L. Lopez, D. V. Nanopoulos, R. Rangarajan, and A. Zichichi, *Light gravitino production at hadron colliders*, *Phys.Rev.* **D57** (1998) 373–382, [[hep-ph/9707331](#)].
- [34] M. Klasen and G. Pignol, *New results for light gravitinos at hadron colliders: Tevatron limits and LHC perspectives*, *Phys.Rev.* **D75** (2007) 115003, [[hep-ph/0610160](#)].
- [35] K. Mawatari and Y. Takaesu, *HELAS and MadGraph with goldstinos*, *Eur.Phys.J.* **C71** (2011) 1640, [[arXiv:1101.1289](#)].
- [36] P. de Aquino, F. Maltoni, K. Mawatari, and B. Oehl, *Light gravitino production in association with gluinos at the LHC*, *JHEP* **1210** (2012) 008, [[arXiv:1206.7098](#)].
- [37] M. Papucci, A. Vichi, and K. M. Zurek, *Monojet versus the rest of the world I: t-channel models*, *JHEP* **1411** (2014) 024, [[arXiv:1402.2285](#)].
- [38] A. Alloul, N. D. Christensen, C. Degrande, C. Duhr, and B. Fuks, *FeynRules 2.0 - A complete toolbox for tree-level phenomenology*, *Comput.Phys.Commun.* **185** (2014) 2250–2300, [[arXiv:1310.1921](#)].
- [39] R. Casalbuoni, S. De Curtis, D. Dominici, F. Feruglio, and R. Gatto, *A gravitino - goldstino high-energy equivalence theorem*, *Phys.Lett.* **B215** (1988) 313.
- [40] R. Casalbuoni, S. De Curtis, D. Dominici, F. Feruglio, and R. Gatto, *High-energy equivalence theorem in spontaneously broken supergravity*, *Phys.Rev.* **D39** (1989) 2281.
- [41] D. Volkov and V. Soroka, *Higgs effect for goldstone particles with spin 1/2*, *JETP Lett.* **18** (1973) 312–314.
- [42] S. Deser and B. Zumino, *Broken supersymmetry and supergravity*, *Phys.Rev.Lett.* **38** (1977) 1433.
- [43] K. Mawatari and B. Oehl, *Monophoton signals in light gravitino production at e^+e^- colliders*, *Eur.Phys.J.* **C74** (2014) 2909, [[arXiv:1402.3223](#)].
- [44] H. Baer, K.-m. Cheung, and J. F. Gunion, *A Heavy gluino as the lightest supersymmetric particle*, *Phys.Rev.* **D59** (1999) 075002, [[hep-ph/9806361](#)].

- [45] Y. Kats, P. Meade, M. Reece, and D. Shih, *The status of GMSB after 1/fb at the LHC*, *JHEP* **1202** (2012) 115, [[arXiv:1110.6444](#)].
- [46] J. Alwall, C. Duhr, B. Fuks, O. Mattelaer, D. G. Ozturk, et al., *Computing decay rates for new physics theories with FeynRules and MadGraph5_aMC@NLO*, [arXiv:1402.1178](#).
- [47] N. D. Christensen, P. de Aquino, C. Degrande, C. Duhr, B. Fuks, et al., *A Comprehensive approach to new physics simulations*, *Eur.Phys.J.* **C71** (2011) 1541, [[arXiv:0906.2474](#)].
- [48] C. Degrande, C. Duhr, B. Fuks, D. Grellscheid, O. Mattelaer, et al., *UFO - The Universal FeynRules Output*, *Comput.Phys.Commun.* **183** (2012) 1201–1214, [[arXiv:1108.2040](#)].
- [49] P. de Aquino, W. Link, F. Maltoni, O. Mattelaer, and T. Stelzer, *ALOHA: Automatic Libraries Of Helicity Amplitudes for Feynman Diagram Computations*, *Comput.Phys.Commun.* **183** (2012) 2254–2263, [[arXiv:1108.2041](#)].
- [50] J. Alwall, R. Frederix, S. Frixione, V. Hirschi, F. Maltoni, et al., *The automated computation of tree-level and next-to-leading order differential cross sections, and their matching to parton shower simulations*, *JHEP* **1407** (2014) 079, [[arXiv:1405.0301](#)].
- [51] T. Sjostrand, S. Mrenna, and P. Z. Skands, *PYTHIA 6.4 Physics and Manual*, *JHEP* **0605** (2006) 026, [[hep-ph/0603175](#)].
- [52] **DELPHES 3** Collaboration, J. de Favereau et al., *DELPHES 3, A modular framework for fast simulation of a generic collider experiment*, *JHEP* **1402** (2014) 057, [[arXiv:1307.6346](#)].
- [53] E. Conte, B. Fuks, and G. Serret, *MadAnalysis 5, A user-friendly framework for collider phenomenology*, *Comput.Phys.Commun.* **184** (2013) 222–256, [[arXiv:1206.1599](#)].
- [54] J. Pumplin, D. Stump, J. Huston, H. Lai, P. M. Nadolsky, et al., *New generation of parton distributions with uncertainties from global QCD analysis*, *JHEP* **0207** (2002) 012, [[hep-ph/0201195](#)].
- [55] W. Beenakker, R. Hopker, M. Spira, and P. Zerwas, *Squark and gluino production at hadron colliders*, *Nucl.Phys.* **B492** (1997) 51–103, [[hep-ph/9610490](#)].
- [56] D. Goncalves-Netto, D. Lopez-Val, K. Mawatari, T. Plehn, and I. Wigmore, *Automated squark and gluino production to next-to-leading order*, *Phys.Rev.* **D87** (2013) 014002, [[arXiv:1211.0286](#)].
- [57] M. Cacciari, G. P. Salam, and G. Soyez, *The Anti- $k(t)$ jet clustering algorithm*, *JHEP* **0804** (2008) 063, [[arXiv:0802.1189](#)].
- [58] J. Alwall, S. de Visscher, and F. Maltoni, *QCD radiation in the production of heavy colored particles at the LHC*, *JHEP* **0902** (2009) 017, [[arXiv:0810.5350](#)].
- [59] C. Petersson, A. Romagnoni, and R. Torre, *Higgs decay with monophoton + MET signature from low scale supersymmetry breaking*, *JHEP* **1210** (2012) 016, [[arXiv:1203.4563](#)].
- [60] M. Cacciari, G. P. Salam, and G. Soyez, *FastJet user manual*, *Eur.Phys.J.* **C72** (2012) 1896, [[arXiv:1111.6097](#)].